Analysis and Prediction of Cirrus-Top Altitude and Ice Water Path in a Mesoscale Area

DONALD C. NORQUIST

Air Force Research Laboratory, Hanscom Air Force Base, Massachusetts

ROBERT P. D'ENTREMONT

Atmospheric and Environmental Research, Inc., Lexington, Massachusetts

(Manuscript received 10 October 2001, in final form 17 February 2003)

ABSTRACT

Vertical distributions of clouds have been a focus of many studies, motivated by their importance in radiative transfer processes in climate models. This study examines the horizontal distribution of cirrus clouds by means of satellite imagery analyses and numerical weather prediction model forecasts. A ground-truth dataset based on two aircraft mission periods flying particle probes through cirrus over a ground-based cloud radar is developed. Particle probe measurements in the cirrus clouds are used to compute ice water content and radar reflectivity averages in short time periods (25–30 s). Relationships for ice water content as a function of reflectivity are developed for 6-K ambient temperature categories. These relationships are applied to the radar-measured short-term-averaged reflectivities to compute vertical profiles of ice water content, which are vertically integrated over the depth of the observed cirrus clouds to form ice water path estimates. These and cloud-top height are compared with the same quantities as retrieved by the Geostationary Operational Environmental Satellite (GOES) level-2B algorithm applied to four channels of *GOES-8* imagery measurements. The agreement in cloud-top height is reasonable (generally less than 2-km difference). The ice water path retrievals are smaller in magnitude than the radar estimates, and this difference grows with increasing cirrus thickness. Comparisons of a sequence of the fifth-generation Pennsylvania State University–National Center for Atmospheric Research Mesoscale Model (MM5) predictions and GOES level-2B retrievals of ice cloud tops for the convectively active second mission period showed that the MM5 cirrus areal extent was somewhat greater than the GOES depictions. Cloud-top height ranges were similar. MM5 is capable of producing ice water path magnitudes similar to the radar estimates, but the GOES retrievals are much more limited. Ninety-eight percent of the GOES grid points had ice water paths no greater than 60 g m^{-2}, as compared with 74% for MM5. Ten percent of MM5 points had ice water content >200 g m^{-2}, as compared with 0.07% for GOES retrievals. Based on this study, we conclude that GOES level-2B cloud-top retrievals are a reliable tool for prediction evaluations but the algorithm's retrievals of ice water path are not.

1. Introduction

Interest in cirrus clouds and their impact on radiant energy transfer has grown with the focus on climate modeling to assess greenhouse warming of the earth's atmosphere. This interest has motivated many studies of the characteristics of cirrus clouds to better understand their nature and evolution so that they can be modeled or parameterized in the models.

No single observing system can measure all of the important characteristics of cirrus clouds. Satellite-based remote sensing can provide images of large areas of cirrus, and the radiation emitted by cirrus can be measured and used to estimate certain geometric and microphysical properties. Combinations of active and passive ground-based remote sensors have been used to measure or deduce a number of microphysical quantities, including ice water content (IWC), in the limited area subject to their observational reach. Aircraft carrying particle probes can traverse cirrus clouds to obtain direct measurements from which the concentrations, shapes, and sizes of ice crystals can be obtained but such sampling is temporally and spatially limited. Thus, it is necessary to try to exploit the complementary strengths of the various cirrus-observing systems to spatially and temporally characterize the clouds.

Studies involving satellite retrievals of the ice water path (IWP) have primarily involved microwave rather than infrared wavelength radiation measurements. Liu

Corresponding author address: Donald C. Norquist, AFRL/VSBL, 29 Randolph Rd., Hanscom AFB, MA 01731-3010.
E-mail: donald.norquist@hanscom.af.mil

and Curry (1998) used airborne millimeter-wave imaging radiometer measurements at 150 and 220 GHz to retrieve estimates of IWP and at lower frequencies to determine background radiation from underlying liquid water clouds. They compared selected retrievals with IWP inferred from collocated aircraftborne particle probe measurements and found good agreement, given the incompatibility of the volume average of the satellite and point measurements of the probes. Liu and Curry (1999) then used observations from the Defense Meteorological Satellite Program's Special Sensor Microwave (SSM) water vapor sounder to retrieve IWP in cirrus clouds over ocean areas. They linked IWP to relative values of the 150-GHz brightness temperature, correcting for the effect from liquid water path (LWP) using SSM Imager (SSM/I) data and relative humidity analysis profiles. IWP retrievals were compared with International Satellite Cloud Climatology Project (ISCCP) analyses. They found that IWP tends to increase with decreasing cloud-top temperature, especially for precipitating clouds.

Liu and Curry (2000) used the same datasets to simultaneously retrieve IWP and mass median particle diameter from nonprecipitating cirrus using a lookup table developed from a series of executions of a radiative transfer model. Lookup table entries depended on cloud types (relative amounts of liquid and ice water), cloud LWP, and temperature and humidity profiles. They found that the simultaneous retrieval scheme is limited in its applicability to clouds with IWP > 200 g m^{-2} and mass median particle diameter >200 μm. Higher microwave frequencies are needed for thinner cirrus clouds.

Sheu et al. (1997) used visible and infrared data from ISCCP and microwave brightness temperatures from the SSM/I to estimate IWP over tropical oceans. IWP was derived by one of several methods depending on classification of the cloud, including ISCCP ice optical depth, a retrieval algorithm based on high SSM/I frequencies, and a residual method that difference the ISCCP total optical depth and the SSM/I-derived LWP.

No previous studies of actual IWP retrieval based solely on infrared satellite-sensed radiation were found. However, Stubenrach et al. (1999) used radiation measurements from the 19 infrared channels of the high-resolution infrared radiation sounder (HIRS) aboard the National Oceanic and Atmospheric Administration (NOAA) polar-orbiting environmental satellites to estimate ice crystal size in cirrus clouds. Inversion algorithms were used to estimate brightness temperatures to compute the emissivity of the cirrus at 8.3 and 11.1 μm, after scattering contributions were removed. The ratio of the emissivities was then used to estimate mean ice crystal size with a lookup table produced by a series of executions of a radiative transfer model.

Active and passive ground-based remote sensors have been used in various combinations to infer various cirrus cloud microphysical properties. This type of study has been reported by, for example, Matrosov (1997) and Sekelsky et al. (1999). Matrosov (1997) used Doppler radar and infrared radiometer observations of cirrus clouds in several field experiments to infer cloud thickness, particle size distribution, particle concentration, and IWC. He found considerable variability from cloud to cloud in the parameters used to retrieve cloud properties and measured radar reflectivities on which they are based. The use of reflectivity of greater magnitudes was found to reduce this variability. Mace et al. (1998) and Hogan et al. (2001) compared NWP model predictions of vertical cloud structure at a single model grid box with ground-based remote sensor observations of the clouds over seasonal time periods.

Cirrus microphysical measurements by aircraftborne particle probes were utilized to assess particle concentrations by size categories, IWC, radar reflectivity, and effective particle diameter in studies reported by Brown et al. (1995), Atlas et al. (1995), McFarquhar and Heymsfield (1996), and Liu and Illingworth (2000). These studies involved the analysis of ice crystal measurements from several field experiments that involved tropical and midlatitude cirrus clouds. Several of the studies empirically derived relationships between IWC and radar reflectivity from scatterplots of the two quantities computed from the particle probe measurements. Young et al. (1998) compared the particle probe assessments with similar quantities retrieved from satellite imagery.

In this paper we demonstrate how the complementary strengths of the different cirrus observing and prediction systems can be used to obtain cirrus altitudes and IWP over large areas and short time intervals. We begin with the direct measurements of cirrus particle concentrations by aircraftborne particle probes to compute IWC and equivalent radar reflectivity (Z_e). Best-fit IWC–Z_e relationships are then applied to reflectivity measurements of a cloud radar operating in the same vicinity to obtain vertical profiles of IWC and top and base altitude for each cirrus layer. The radar-derived IWC in the topmost layer is integrated to obtain IWP. Radar IWP and top altitude are compared with IWP retrieved from geostationary satellite imagery at the radar site. Last, mesoscale NWP model predictions of IWC are integrated and the IWP and top altitude are compared with satellite-retrieved IWP and top altitude over a mesoscale area.

2. Description of the data

Airborne particle probe, ground-based cloud radar, and satellite imagery data were collected during a cirrus cloud field experiment based at Everglades City, Florida, in September 1996. Figure 1 shows the temporal extent of the datasets used for each of the three major data sources. The following sections discuss the observation systems and their measurements.

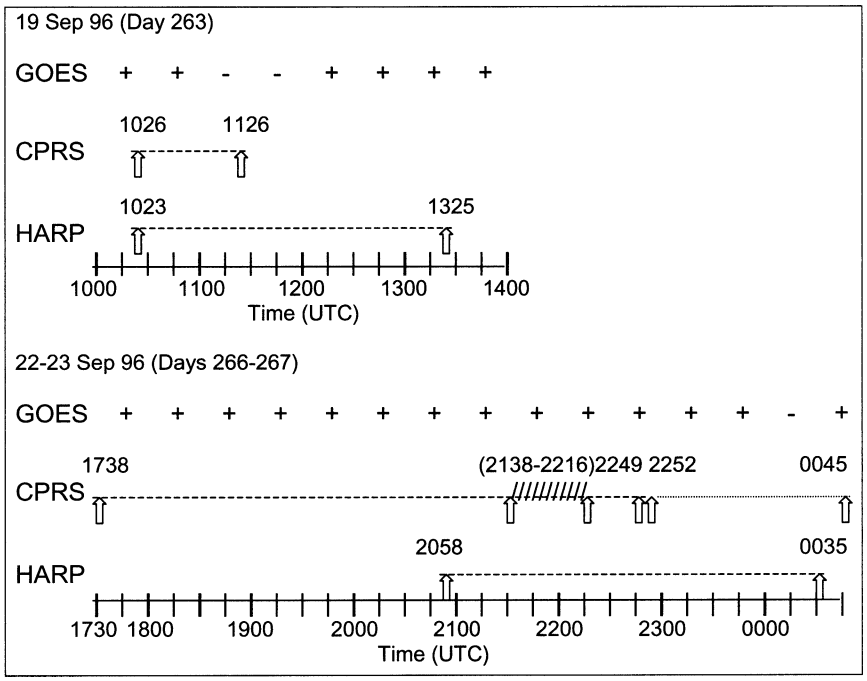

FIG. 1. Coincident observational datasets available for use in this study. *GOES-8* imagery data were available (+) and missing (−) at the indicated times. Arrows and times indicate start and stop times of the CPRS and HARP measurements for both missions. For CPRS, the zenith mode (dashed line) and scan mode (dotted line) times are indicated; convection (slashes) occurred over the radar site, and so CPRS observations were not used.

a. HARP particle probe measurements

Three particle probe systems for collecting and measuring ice crystals were a part of the instrument package of the Aeromet, Inc., High-Altitude Reconnaissance Platform (HARP) aircraft (Morrison et al. 1997) during the field experiment. Ice particle concentrations were reported by size bin using a 1) forward scattering spectrometer probe (FSSP), for seven 6-μm-wide bins from 6 to 48 μm; 2) one-dimensional optical array probe (1D-C), for fourteen 20-μm-wide bins from 20 to 300 μm and one +300 μm bin; and 3) two-dimensional optical array probe (2D-C), for thirty-one 25-μm-wide bins from 25 to 800 μm and one +800 μm bin.

Of the three probes, the 2D-C has the advantage of measuring the particles's dimensions parallel and perpendicular to the flight path. Because the 1D-C and 2D-C probes have nearly the same size range through 300 μm, we did not include the 1D-C measurements in this study. Brown et al. (1995) and McFarquhar and Heymsfield (1996) have stated that at an airspeed of 200 m s^{-1}, the 2D-C does not reliably measure particles smaller than about 100 μm. Because HARP aircraft averaged airspeeds of about 150 m s^{-1} during the Everglades City missions, the 75–100-μm bin was included in the processing. The contribution of the smaller particles measured by the FSSP to the total IWC was evaluated by Brown et al. (1995) and McFarquahar and Heymsfield (1996) and found to be small (less than 20%) especially for larger IWCs. A similar assessment of the FSSP's contribution is conducted in this study.

An available two-dimensional precipitation (2D-P) probe was not flown in the Everglades City missions. Liu and Illingworth (2000) give the range of this probe as 200–6400 μm. McFarquhar and Heymsfield (1996) analyzed three missions that traversed tropical cirrus anvils. They did not use the 2D-P data because the ice particles were not measured well by the probe, but did show 2D-C particle concentrations for particles >1000 μm. The presence of some particles >1000 μm is likely in the cirrus anvil clouds observed in the Everglades City missions. Particles in the range 1000–6400 μm were accounted for by extrapolating the 2D-C particle concentrations out to these particle sizes as described in section 3.

The HARP aircraft flew racetrack loops over the study area at varying altitudes between 6.6 and 12.2 km. The long legs of the flight-track loops were aligned with the prevailing wind direction. The flight track never took the aircraft more than 35 km from the location of the ground-based sensors. On each loop the aircraft flew over the location of the ground-based sensors. Because the prevailing wind speeds at flight levels averaged about 50 km h^{-1}, the ground sensors saw 150–200-km spans of clouds as they were advected by the observing site. Thus, the aircraft and ground sensors were sampling generally the same cloud environment. The air-

craft also measured atmospheric state variables, including temperature and wind speed, that were used in the processing of the data in this project.

b. CPRS cloud radar measurements

Observations of reflectivity of the radar signal from the cirrus particles were made by the Cloud Profiling Radar System (CPRS) of the University of Massachusetts (Sekelsky et al. 1999). For the September 1996 field experiment, the CPRS radar and other ground-based sensors were located at 25.85°N, 81.38°W near Everglades City. The CPRS is a dual-frequency cloud radar system, with Ka-band frequency of 33 GHz (9.06-mm wavelength) and W-band frequency of 95 GHz (3.16-mm wavelength). The minimum detectable reflectivity is −63 and −59 dBZ, respectively, for a range of 1 km and 30 s averaging. The CPRS can be operated in zenith (straight up) or scan (fixed azimuth, changing elevation) mode. In the zenith mode, the prevailing wind speed and direction can be used to advect cloud particles across the beam path, resulting in a 1 dimensional time series of cloud measurements. In scan mode, the scan plane is oriented perpendicular to the prevailing wind direction, allowing a time series of pie-shaped swaths of measurements. The nominal range interval is 75 m, and the nominal time interval between measurements is 10–40 s.

c. GOES-8 satellite imagery

Radiance data from all available channels of the imagery sensor on board the *Geostationary Operational Environmental Satellite* (*GOES*)*-8* operated by NOAA were used to perform retrievals of certain cirrus properties. The *GOES-8* satellite orbits the earth in a fixed geostationary position, located at 75°W longitude over the equator. Imagery data were available for the entire field of view of the satellite at 15 and 45 min past each hour (UTC). The data are archived routinely on the Air Force Research Laboratory Interactive Meteorological System at Hanscom Air Force Base, Massachusetts.

The retrieval process used to obtain the cirrus cloud properties is referred to as the GOES level-2B algorithm (Gustafson and d'Entremont 2000). While the algorithm uses all available imagery channels to generate a cloud mask, it is designed to perform the retrievals using GOES thermal infrared bands of wavelengths 3.9, 6.7, 10.7, and 12 μm. It provides estimates of cirrus cloud spatial (cloud fraction, effective cloud-top height/pressure/temperature), radiative (effective emissivity at each thermal infrared band, visible optical thickness), and microphysical (ice crystal effective diameter, IWP) properties. Only cloud-top height (CTH) and IWP retrievals were utilized in this study. The grid spacing of the pixels for which the retrieved properties are provided is approximately 4 km at nadir. The GOES level-2B algorithm is described in more detail by Gustafson and d'Entremont (2000).

d. Description of cirrus cloud conditions

During September strong tropical convection is common in southern Florida and surrounding waters. On 19 September broken patches of heavy cirrus moved through the area and were sampled by the HARP aircraft and the CPRS radar during the period 1026–1126 UTC. At that point, the CPRS was switched from zenith to scan mode and scans were executed during the period 1128–1530 UTC. Unfortunately, the scan-mode data were unrecoverable upon later processing and were not available for this project. At about 1230 UTC a cumulonimbus cloud developing northwest of Everglades City was producing anvil cirrus that was drifting toward the ground-based sensor site. By 1300 UTC thick anvil cirrus was over the site, and the particle probes on the HARP aircraft measured appreciable ice particle concentrations at 10–11-km altitude until it began its descent at about 1330 UTC.

On 22 September at about 2015 UTC, cirrus from a nearby convective cell began drifting over the site and was observed by the CPRS radar. By the time of the arrival of the HARP aircraft in the study area at about 2100 UTC, the anvil cirrus was widespread and several kilometers thick. HARP observed appreciable particle concentrations at 8–9-km altitude and the CPRS Ka-band radar measured reflectivities as high as −3 dBZ from 7 to 10 km. At 2315 UTC, anvil cirrus appeared over the ground-based sensor site from a line of diminishing convection oriented east–west across southern Florida. The cirrus grew increasingly thick until cessation of CPRS scanning at 0045 UTC 23 September. Particle probes taking measurements at 8–13-km altitude between 2315 and 0035 UTC observed heavy particle concentrations.

3. Method

a. HARP particle probe measurements

The observed particle concentrations measured by the FSSP and 2D-C at approximately 1-s intervals were averaged by size bin over the time required for the aircraft to traverse a GOES imagery pixel. The average dimension of a GOES pixel in the region of interest in this study was 3.55 km, which at typical aircraft speeds resulted in averaging periods of 25–30 s. This averaging was done to ensure that the particle concentrations used to compute IWC vs Z_e relationships were representative of the length scales over which they would be applied. The averages were computed only for periods in which the aircraft's altitude was greater than 6 km for the duration of the averaging period. Time-averaged particle concentrations by size bin were computed for a total of 1126 averaging periods during the two HARP missions

whose durations are depicted in Fig. 1. The time-averaged particle concentrations for the 30 2D-C size bins were used in the computations of IWC and Z_e discussed next.

Liu and Illingworth (2000) show that accurate and realistic computations of IWC and Z_e can be obtained when the density of the ice particles is assumed to vary with effective particle diameter D_i (taken as the calibrated bin size for each 2D-C bin i):

$$\text{IWC} = \frac{\pi}{6}\sum_{i=1}^{n}\rho_i N_i D_i^3, \tag{1}$$

$$Z_e = |K_w|^{-2}\sum_{j=1}^{n}|K_i|_j^2 N_j D_j^6 f(D_j, \rho_j), \tag{2}$$

where $\rho = 0.07\,D^{-1.1}$ (ρ is in grams per centimeter cubed and D is in millimeters; $\rho = 0.916$ g cm^{-3} is used for particles that have a diameter of 0.1 mm or less), as recommended by Liu and Illingworth (2000). The time-averaged particle concentrations in the $n = 30$ 2D-C size bins were used as the values for N_i in (1) and (2) to compute IWC (g m^{-3}) and Z_e (mm^6 m^{-3}) for each averaging period. A dimensionless quantity K is given by

$$K = \frac{m^2 - 1}{m^2 + 2}, \tag{3}$$

where m is the complex index of refraction for the observed media (cloud water droplets or ice particles). Sekelsky et al. (1999) gives $|K_w|^2$ values of 0.885 and 0.698 for 33 and 95 GHz, respectively. According to Gardiner and Hallett (1985), (3) can be expressed for ice particles as

$$K_i = \frac{e - 1}{e + 2}; \tag{4}$$

where $e = m^2$ and is defined as

$$e = \frac{1 + f_0(Be_0 - 1)}{1 + f_0(B - 1)}; \tag{5}$$

where $f_0 = \rho/0.916$, $f_0 \le 1$, and ρ is the ice density in g cm^{-3},

$$B = \left(\frac{2}{e_0 - 1}\right)\left[\left(\frac{e_0}{e_0 - 1}\right)\ln e_0 - 1\right], \tag{6}$$

and $e_0 = e$ for solid ice at a specified radar reflectivity. To determine e_0 for radar frequencies of 33 and 95 GHz, we substitute e_0 into (4) and solve for e_0. Sekelsky et al. (1999) gives values of $|K_i|^2 = 0.176$ for solid ice for both radar frequencies, and so using $K_i = \sqrt{0.176}$ yields $e_0 = 3.172$ and $B = 0.632$, which, in (5), gives

$$e = \frac{1 + 1.005 f_0}{1 - 0.368 f_0}. \tag{7}$$

Thus, for radar frequencies of 33 and 95 GHz, $|K_i|^2$ in (2) is a function of ice density only (which in turn is dependent only on particle diameter) and is computed from (4) and (7).

Liu and Illingworth (2000) include the ratio of scattering of the radar signal as given by the Mie scattering model to that of the Rayleigh scattering model in (2) as the factor $f(D_i, \rho_i)$. The backscatter efficiency according to the Rayleigh model is given by Sekelsky et al. (1999) and Bohren and Huffman (1983) as

$$\xi_R = 4\pi^4\lambda^{-4}D^4|K_i|^2,$$

where λ is the wavelength of the electromagnetic signal. The Rayleigh backscatter can then be computed for each calibrated particle size (D_i, in millimeters) separately for each wavelength simply by using the $|K_i|^2$, whose computations are described above. The backscatter efficiencies of small ice spheres by the Mie scattering model were calculated using the routine BHMIE as adapted from Bohren and Huffman (1983). As with the Rayleigh computations, the Mie backscatter efficiency is computed for each calibrated particle size separately for each wavelength, using the refractive index $m = \sqrt{e}$ where e is obtained from (7) for each particle size bin.

The time-averaged 2D-C particle concentrations of the two mission periods used in (1) and (2) resulted in 601 time-averaged particle size spectra with nonzero IWC and Z_e greater than -40 dBZ. These are shown in a scatterplot for the Ka-band radar frequency (33 GHz) in Fig. 2. Also shown in Fig. 2 is a best-fit power-law relationship in the form IWC $= aZ_e^b$, derived from the data. Equivalent reflectivity is displayed in dBZ units, defined as dB$Z = 10\log_{10} Z_e$. The scatterplot and power-law relationship for the W-band frequency (95 GHz) were very similar, yielding only a slightly smaller value of IWC for a given value of Z_e.

There are several potential sources of uncertainty in the computations of IWC and Z_e from (1) and (2). First is the relationship used for the density of the particles. Liu and Illingworth (2000) computed values of IWC and Z_e for several formulations of the ice density assumption. For those formulations that yielded IWC in good agreement with directly measured IWC, they found differences in IWC as large as 30% for values of IWC ≥ 0.1 g m^{-3}. Brown et al. (1995) showed that observations of the 2D optical array probe, processed using the $D^{-1.1}$ density formulation, were in good agreement with IWC derived from a total water content probe. The second potential uncertainty is determination of particle size. In the HARP 2D-C, the particle dimension parallel to the diode array (the Y dimension) was used to represent particle diameter because its calibration is not affected by aircraft speed. Brown et al. (1995) used the mean of the parallel and perpendicular (X) dimension of the particles to determine diameter in midlatitude clouds, but used the Y dimension in tropical cirrus. Atlas et al. (1995) determined particle size as the maximum projection of the particle, either X or Y, whichever was larger. They then estimated the equivolume diameter by

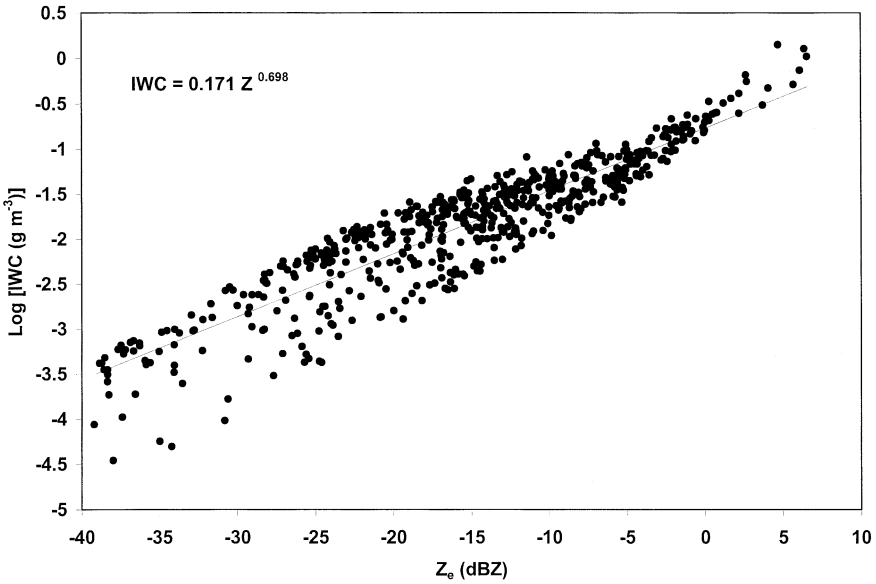

FIG. 2. IWC vs Z_e computed for 601 short-time averages of 2D-C particle concentrations by size bin for the HARP aircraft mission periods shown in Fig. 1. These values are computed from (1) and (2) with a radar frequency of 33 GHz. The best-fit power-law relationship is shown by the straight line plotted through the points and is given by the formula in the figure.

multiplying the maximum projection by 0.8. McFarquhar and Heymsfield (1996) calculated IWC from tropical anvil cirrus particles using categories of maximum size and area ratio (particle area/area of circumscribed circle) and found that the values from the two approaches agreed within a factor of 2. Gayet et al. (1993) showed that for a set of different probes, particle size is within 10% of each other but concentrations can be as different as 150%. This leads to the third uncertainty issue, which is the determination of particle concentration. There are two factors involved in this issue: the determination of sample volume and the rejection of particles by the probe. Sample volume was determined in the HARP 2D-C processing as a function of particle size and sampling speed, following Baumgardner and Korolev (1997). This approach represents a significant improvement over the probe manufacturer's recommended method. Several tests are used for particle acceptance. If a particle was collected too closely in time to the previous particle to have likely come from a Poisson distribution of the mean particle concentration, the latter particle is rejected. This rejects fragments of particles that are shattered by the probe. Also rejected were particles based on their X and Y dimensions, for example if $X > CY$ then the particle would be rejected, where C is an arbitrary but sensible number, like 10. Last, there is also some possibility that the aircraft wing tip vortices systematically rotate the particles before they are sampled and, thus, causes a bias in how they are sized. A visual inspection of thousands of images suggested that this did not appear to be a problem.

Equations (1) and (2) were also applied to the time-averaged FSSP concentration in six size bins in the range 12–48 μm. Because density is a maximum for these small particles, IWC can be appreciable for large concentrations of such particles (Brown et al. 1995; McFarquhar and Heymsfield 1996). However, particles of such small size do not contribute significantly to the measured reflectivity. To determine the relative contribution to total IWC, we computed the ratio $\mathrm{IWC}_{\mathrm{FSSP}}/\mathrm{IWC}_{\mathrm{FSSP+2D\text{-}C}}$ for all averaging periods. This ratio was greater than 0.5 for less than 5% of the averaging periods having nonzero 2D-C IWC. Therefore, the FSSP measurements were not included in the development of IWC, Z_e relationships from the particle probe data.

Larger particles have a major impact on reflectivity. No concentrations for particle sizes > 800 μm were included in the particle probe dataset so that particle concentrations were simulated for the 2D-P range 1000–6400 μm. For each averaging period with nonzero IWC, the time-averaged 2D-C particle concentration in each size bin was divided by the bin width (25 μm) to form normalized particle concentration, N^*. A best-fit power-law relationship with bin size D of the form $N^* = cD^d$ was constructed for each time-averaged 2D-C particle spectrum, and then was evaluated at 200-μm intervals from 1000 to 6400 μm inclusive. Our investigation showed that the power-law relationship produced simulated 2D-P particle concentrations that compared better with observations from other studies than an exponential form more commonly associated with the concentration of larger particle sizes (Ryan 2000). A gamma function is commonly used to fit the distribution for the full range of particle sizes but of course actual particle counts in the 2D-P size range were not available to confirm such a distribution. The largest particle concentration of

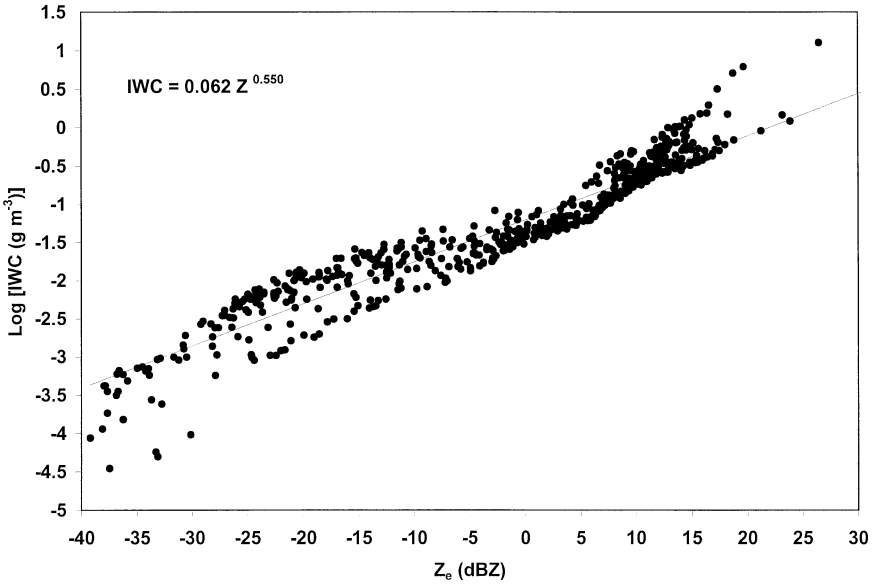

FIG. 3. Same as for Fig. 2, except that simulated 2D-P particle concentrations were included with the measured 2D-C concentrations in the IWC and Z_e computations.

>1000 μm, reported by McFarquhar and Heymsfield (1996), of 0.2 L^{-1} was converted to normalized particle concentration (1.0 m^{-3} μm^{-1}) to act as an upper limit for the simulated values. The simulated N^* for each size bin of a time-averaged spectra was multiplied by 1.0 m^{-3} $\mu m^{-1}/N^*_{1000}$ when $N^*_{1000} > 1.0$ m^{-3} μm^{-1} to proportionately reduce each of the larger particle concentrations below this upper limit. The computed values of normalized concentration were multiplied by 2D-P bin width (200 μm) to form particle concentrations that were used in (1) and (2) to estimate simulated 2D-P IWC and Z_e. Values of total IWC and Z_e (2D-C + simulated 2D-P) are displayed for the 601 2D-C time averages in Fig. 3. Note that these estimates would represent an upper limit to the actual 2D-P particle concentrations had they been measured, because it is unlikely that every 2D-P size bin would have as great a concentration as the simulated value.

It is clear from comparing Figs. 2 and 3 that both IWC and Z_e have increased with the addition of the simulated 2D-P concentrations, especially for time averages with larger (>0.01 g m^{-2}) 2D-C IWC. The ratios $IWC_{2D\text{-}P}/IWC_{2D\text{-}C+2D\text{-}P}$ and $Z_{e2D\text{-}P}/Z_{e2D\text{-}C+2D\text{-}P}$ were computed for the 601 time averages—45% of IWC ratios and 79% of 33 GHz Z_e ratios were >0.5. Thus, the simulated 2D-P concentrations make a significant contribution to the total IWC and Z_e. For any given value of Z_e, the log IWC is 0.3–0.4 lower for the 2D-C + 2D-P values than for the 2D-C values. This is because adding the larger 2D-P particles increases the Z_e more than the IWC because of the very low density of the very large particles. So the computations of IWC from radar reflectivity, based on the 2D-C + 2D-P relationships, should give lower values than those based on the 2D-C only relationships. Using both values will represent bounding values for the radar-inferred IWC. We note that the IWC–Z_e relationships in Figs. 2 and 3 actually do bound the relationships found by Liu and Illingworth (2000), of IWC = 0.097 $Z^{0.59}$, and Atlas et al. (1995), of IWC = 0.064 $Z^{0.58}$, for a comparable radar frequency.

Liu and Illingworth (2000) point out that the general increase in particle size with ambient temperature can be exploited to derive separate IWC–Z_e relationships for stratified temperature regimes. The IWC–Z_e pairs were categorized in 6-K temperature bins using the time-averaged aircraft-measured air temperature. Separate best-fit relationships were computed for each temperature category, separately for 33 and 95 GHz. The resulting scatterplots and best-fit IWC–Z_e relationships for the 2D-C data are shown in Fig. 4 for 33 GHz. Note that too few pairs were available in two of the temperature categories, so values of the parameters of the linear least squares best fit were interpolated or extrapolated from contiguous categories. Temperature category scatterplots and best-fit IWC–Z_e relationships for the 2D-C + 2D-P IWC and Z_e were generated also, but are not shown.

The best-fit lines move down and to the right with increasing ambient temperature. This implies that the use of a single IWC–Z_e relationship to infer IWC from radar data would tend to overestimate IWC at warm temperatures and underestimate IWC at colder temperatures. The root-mean-square error estimate of log IWC from the 33-GHz relationships, when compared with IWC computed from the particle probe measurements, was 0.303 for the single relationship and 0.222 for the temperature-dependent relationships. A similar reduction was observed for the 95-GHz relationships. Liu and

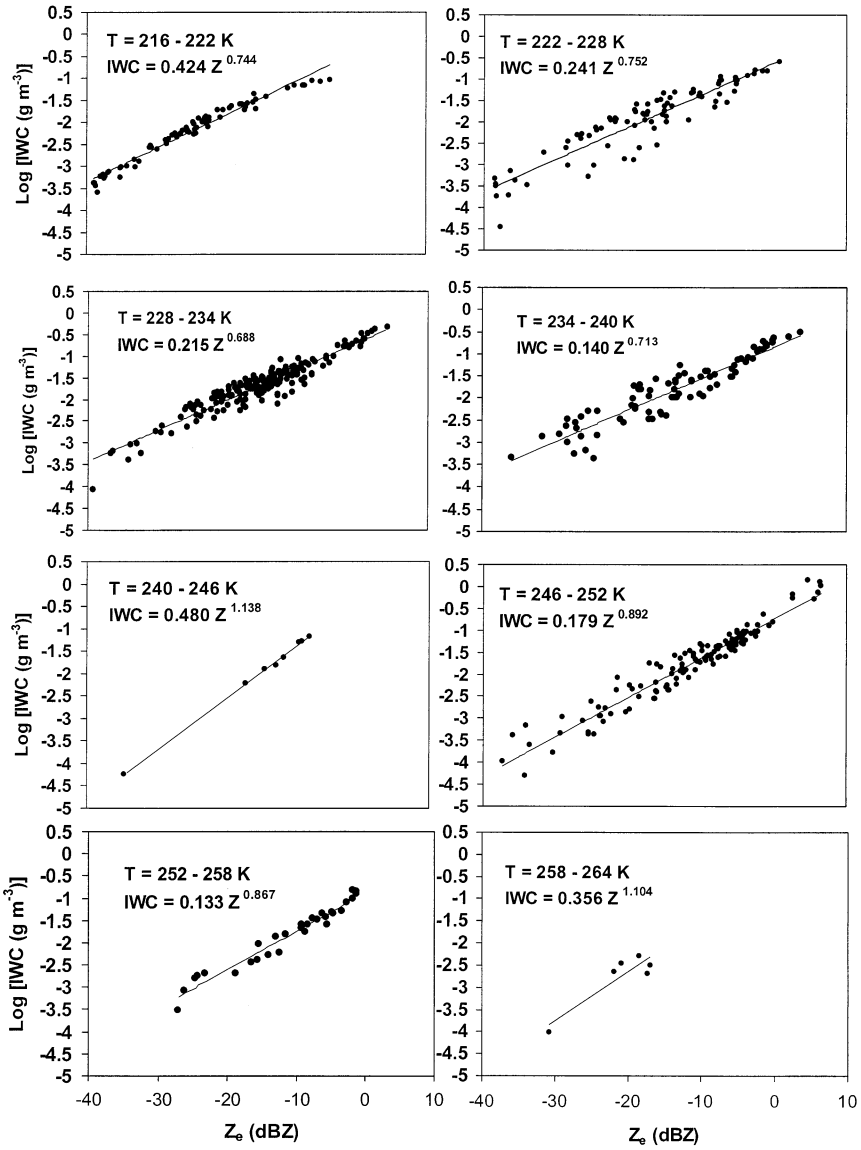

FIG. 4. Ice water content vs equivalent radar reflectivity, categorized by 6-K ambient temperature ranges, for the same 601 short-time averages shown in Fig. 2.

Illingworth (2000) report that errors of 0.3–0.4 were reduced by temperature classification to errors of 0.2–0.3. Therefore, the IWC–Z_e relationships derived from the variable density and temperature category assumptions for 2D-C and 2D-C + 2D-P were applied to reflectivity measurements from cloud radar as described in the following section.

b. CPRS cloud radar measurements

The equivalent radar reflectivity Z_e as measured by the CPRS cloud radar at 33 and 95 GHZ during the time periods indicated in Fig. 1 were processed in a manner similar to the particle probe data. The observed values of Z_e (mm^6 m^{-3}) greater than -40 dBZ at each radar measurement location were averaged over the time duration required for an air parcel to traverse the width of a GOES imagery pixel at the speed of the wind at the location. A rawinsonde sounding taken during the 19 September mission, and two taken during the 22–23 September mission, supplied the wind speed and temperature at each radar measurement altitude. The wind speeds at the altitudes processed (6–18.1 km) varied between 30 and 100 km h^{-1}, which for a pixel width of 3.55 km resulted in averaging times of 2–7 min. The 6-K temperature bin corresponding to the temperature at the radar measurement altitude was identified, and the associated IWC–Z_e relationship derived from the particle probe data was applied to the time-averaged reflectivities at that altitude. This resulted in a computed value of IWC for all of the time-

averaging periods at each radar measurement location. Values of 0 g m^{-3} and -40 dBZ were assigned when there was not at least one Z_e measurement >-40 dBZ observed during the averaging time period at a given radar measurement location.

The computed IWC values were used to compute IWP through the uppermost-observed cloud layer. For each GOES satellite imagery time, the corresponding averaging time period of the CPRS data was identified at each radar measurement location. Then the IWC values for the identified time period were collected and averaged in 75-m altitude bins between 6 and 18.1 km. The highest altitude bin containing a nonzero average IWC was identified as the cloud-top bin. Stepping down from this bin, the bin above the first of two consecutive bins that had a zero-averaged IWC value was deemed the cloud-base bin. IWC at midpoints between the bin levels was computed by averaging the bin IWC between each contiguous pair of bins. A preliminary IWP value was computed as the product of bin-midpoint IWC and bin thickness summed over all contiguous bin pairs from cloud top to base. Then, one-half of the cloud-top bin IWC times the thickness of the bin above the cloud-top bin level plus half the cloud-base bin IWC times the thickness of the bin below the cloud-base bin level, was added to the preliminary IWP value. The CTH was then set as the average of the cloud-top bin altitude and the altitude of the bin above it. The cloud-base height was set as the average of the cloud-base bin altitude and the altitude of the bin below it.

In addition to their use in calculating radar-inferred IWC, the averaged radar Z_e values might be used to validate the computed Z_e values from the particle probe data. However, this was not done in this study because of the differences in observing locus due to differing averaging periods, uncertainty in altitude due to the radar vertical bin depth, and the sampling differences between the two platforms.

c. GOES-8 satellite imagery

Imagery data for *GOES-8* pixels were extracted in a region of interest bounded by approximately 20° and 35°N latitude and 75° and 85°W longitude. There were 356 pixels of the average dimension of 4.74 km in the north–south direction, and 461 pixels of the average dimension of 2.35 km in the east–west direction. Over the area surveyed by the HARP aircraft, the average pixel dimension (average of the average north–south and east–west dimensions) was 3.55 km.

Application of the GOES level 2B algorithm to the pixels in the region of interest at each imagery time involved a sequence of processing steps. First, a ''cloud cover'' routine performs cloud detection at each pixel location using two images 1 h apart, creating a cloud/no cloud mask with regard to all clouds for the second image. Next, a routine called ''clear scene'' operates on the cloud mask to compute ground surface-level clear-scene brightness temperatures for all pixels in the region of interest. These are computed for the four infrared wavelengths (3.9, 6.7, 10.7, and 12 μm) directly for cloud-free pixels, and, via interpolation, for pixels beneath detected clouds. The last routine is ''level 2B,'' which generates the spatial, radiative, and microphysical attributes of the cirrus clouds for the cloudy pixels. A rawinsonde sounding provides the reference pressure, temperature, and geopotential height information to assign the corresponding cloud-top quantities. Retrievals are made for only the highest detected cloud layer. The retrieved parameters evaluated in this study were cirrus CTH and IWP. Values for the pixel whose center-point location was closest to the CPRS radar site were selected for direct comparison with the same parameters estimated from the CPRS radar observations.

In determining IWP for cirrus clouds, emissivity, effective particle size, and radiative temperature are retrieved in a simultaneous solution approach in the GOES level-2B algorithm. IWP is obtained as a by-product of this retrieval scheme. According to Gustafson and d'Entremont (2000), there are several sources of uncertainty in the retrieval process. The assumption that the top-of-atmosphere irradiance at certain wavelengths is the linear sum of clear-sky and cloud-emitted radiation neglects atmospheric attenuation within and above the cloud. This represents a source of error in retrieved radiative temperature, but this should be minimal because water vapor is a weak absorber of the wavelengths (thermal infrared) used in the procedure. Absorption efficiencies for ice crystals used in the procedure have small ($<$10%) errors with respect to Mie theory integrations. Scattering and reflectivity are neglected at the thermal infrared wavelengths, which is expected to have a minimal effect. Homogeneity of particle size distribution within the cloud is assumed, but the error introduced can be reduced if this is set as the average size distribution over the entire cloud. This is equivalent to stating that the IWC at any point in the cloud is constant, so that the IWP is simply the IWC times the depth of the cloud.

Liu and Curry (1998) state that the major uncertainties in retrieving IWP from microwave sensors are linked to not knowing the actual particle size distribution and the possible existence of supercooled liquid water in the cloud. Using historical size distributions can lead to errors of as much as $\pm$50% of the retrieved IWP. They state that simultaneous retrievals of IWP and effective particle size may reduce this uncertainty. Errors due to supercooled liquid water in the ice cloud layer depend on the amount and location, with larger amounts and higher altitudes causing greater IWP underestimation. They estimate that for realistic amounts and locations of supercooled water, the underestimation of IWP is about 30%.

Stubenrauch et al. (1999) state that the primary causes of uncertainty in the retrieval of cirrus emissivity at infrared wavelengths are due to corrections imposed for scattering, use of simultaneously retrieved or monthly average

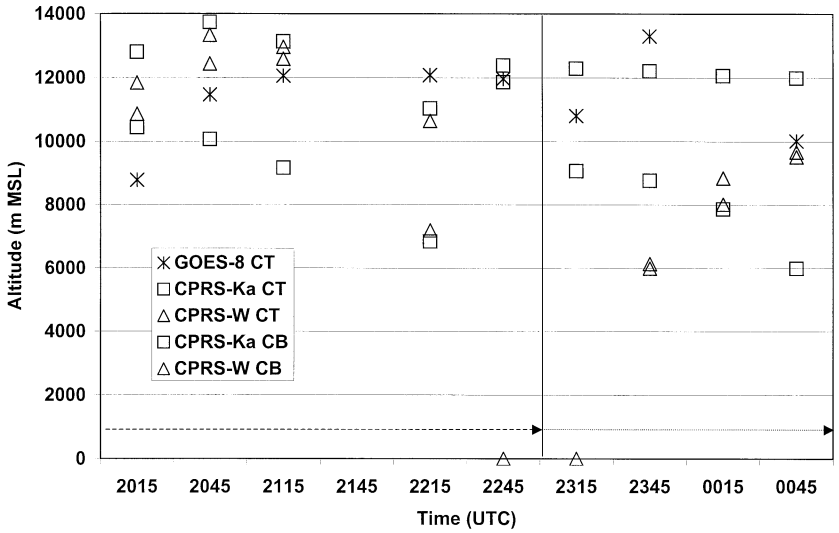

FIG. 5. Comparison of cloud-top (CT) (both *GOES-8* and CPRS Ka and W band) and cloud-base (CB) height (CPRS only) for satellite imagery times on 22–23 Sep 1996 at Everglades City. CPRS in zenith mode (dashed line) and scan mode (dotted line).

temperature and water vapor profiles, the effect of underlying liquid water clouds, and spatial resolution of the retrievals. They found through sensitivity studies that the scattering corrections and spatial resolution are the greatest sources of uncertainty. Errors were as high as ±10% for scattering, especially in regions of small mean median crystal dimension. Where cirrus emissivity was assumed to be heterogeneous (varying pixel to pixel) over a cloud area, as compared with homogeneous, the retrieved mean maximum particle dimension changed by 10%.

4. Results

Figure 5 shows the comparison of CPRS and GOES estimates of CTH for all satellite imagery times between 2015 UTC 22 September and 0045 UTC 23 September for which the GOES imagery data were available. Also included are cloud-base height estimates from the CPRS time-averaged measurements. Application of the 2D-C and the 2D-C + 2D-P IWC, Z_e relationships to radar reflectivity measurements yielded different IWC (thus different IWP) but the same values of cloud-top and -base altitude.

Comparison of the CPRS-estimated cloud-top and -base heights, as shown in Fig. 5, with time–height CPRS reflectivity charts obtained from the field experiment data archive (not shown) showed good agreement of the top and base height positions. There is a noticeable difference in the top and base positions as detected by the Ka- and W-band radar. At 2015–2115 UTC, the cloud layer as depicted by the W band is much thinner than the Ka-band depiction. The thickness are more alike at 2215 UTC, and no cloud is seen at all by the W band at 2245 UTC as compared with a very thin layer observed by the Ka band. The greater sensitivity to the cirrus by the Ka-band radar is in part due to less absorption of the signal with altitude as noted by Sekelsky et al. (1999), by a factor of about 3 for a tropical sounding, and Hogan et al. (2001). The time–height CPRS reflectivity charts for the Ka and W bands confirmed that much more of the cloud cross section was detected by the Ka-band radar. Ka-band radar is more sensitive to the significant amount of Mie scattering by ice particles at cirrus altitudes (Sekelsky et al. 1999), and, thus, is a better standard against which to evaluate cirrus retrieval or prediction methods.

Figure 5 shows that during the zenith-mode sampling period of the 22–23 September mission period, the tendency of the GOES level-2B algorithm to underestimate CTH decreased with time. The Ka-band cloud-top and -base heights show the cloud layer thickening from 2015 to 2115 UTC and remaining thick, but lower, at 2215 UTC. The fact that the GOES level-2B retrieved tops are more accurate when the actual layer is thicker makes sense because the cloud would be less transmissive of upwelling radiation from below. During the scan-mode sampling period, while the cirrus layer is becoming increasingly thick, the GOES level-2B retrievals are within 2 km of the Ka-band cloud-top estimates.

Figure 6 shows a comparison of the IWP from GOES retrievals and Ka-band radar (applying both the 2D-C and 2D-C + 2D-P relationships). The results for the W band are not shown because of the aforementioned greater sensitivity of the Ka band signal at cirrus altitudes. As expected, the CPRS (2D-C + 2D-P) IWP is less than the corresponding CPRS (2D-C) value at most observation times, as are the GOES retrieval estimates. The GOES retrievals appear to be much more steady with time than the radar estimates. Only at 2245 UTC is the GOES estimate of IWP greater than both the CPRS values, which is when, according to Fig. 5, the CPRS found the cloud layer to be very thin. There appears to

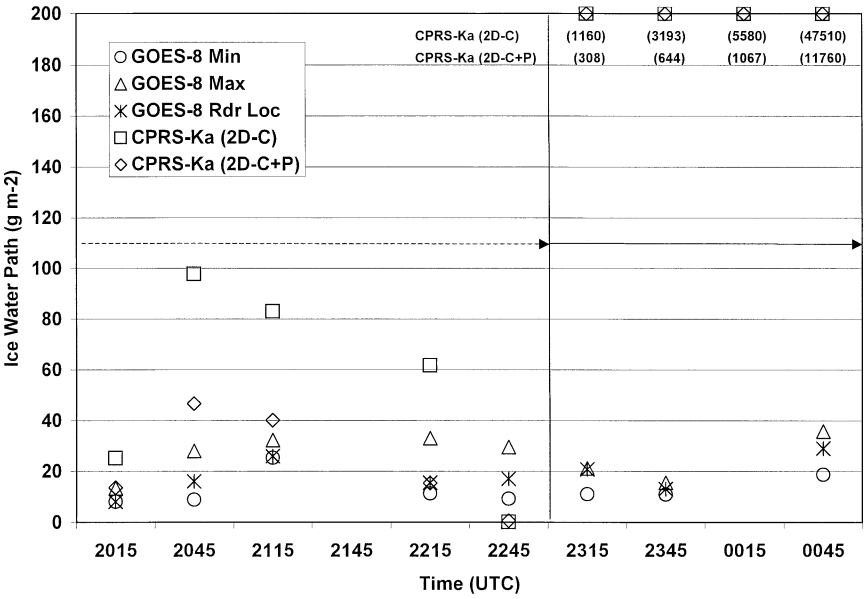

FIG. 6. Comparison of ice water path for the minimum (Min), maximum (Max), and radar location (Rdr Loc) of a 3 × 3 set of *GOES-8* imagery pixels centered at the radar location, and as estimated from the CPRS Ka-band reflectivities for satellite imagery times on 22–23 Sep 1996 at Everglades City. CPRS zenith mode (dashed line) and scan mode (dotted line).

be a consistency between cloud-layer thickness and IWP magnitude in the Ka-band results. When the cloud layer grows increasingly thicker from 2315 to 0045 UTC, the CPRS IWP values are also steadily increasing, while the GOES retrievals are significantly underestimated.

A likely cause of the underestimate of IWC of thick cirrus by the satellite retrieval algorithm is the microphysical structure of the cloud layer. Smaller particle sizes generally dominate the top of a thick cirrus layer where temperatures are colder, while larger particle sizes are found in the warmer temperatures near the layer base. The smaller particles on top have a greater total surface area, so they can effectively absorb the radiation emitted from the larger lower particles and re-emit to space at their colder temperature. Thus, the dominant signal seen by the satellite is from the smaller particles on top, leading to an underestimate of the mean particle size of the layer and a consequent underestimate of the IWP. Radar-derived IWP would generally act as an upper bound on the satellite-retrieved IWP. The greater the cloud thickness, the more likely that satellite IWP $<$ radar IWP. Results from the scan-mode portion of the comparison in Fig. 6 are likely an extreme example of this phenomenon.

5. Comparison of NWP model-predicted cirrus with satellite retrievals

The fifth-generation Pennsylvania State University–National Center for Atmospheric Research (NCAR) Mesoscale Model (MM5; Dudhia 2000) was configured with an inner domain set by the four corner latitude–longitude coordinates of the satellite imagery region of interest. The gridpoint spacing of the inner MM5 domain was set to the mean grid spacing of the GOES pixels, 3.616 km. The inner domain was centrally positioned in an outer domain with 3 times the grid spacing (10.848 km). Forty-one model sigma layers extending from the surface to the model-top pressure (ptop) of 50 hPa were used in both domains, where sigma is defined by $(p - p_{\text{top}})/(p_{\text{sfc}} - p_{\text{top}})$. The surface pressure ($p_{\text{sfc}}$) was derived from the analysis of pressure (p) levels using the gridpoint terrain heights. The mixed-phase explicit moisture scheme (option 3 in Reisner et al. 1998) parameterized the cloud and precipitation microphysical processes in both domains, while the Grell (1993) cumulus parameterization scheme was used in the outer domain only.

The mixed-phase microphysics scheme involves prognostic equations for cloud liquid and ice water and precipitate liquid and ice water. Only the predicted cloud ice water is processed in this study to infer IWP, as described below. Uncertainties in the ice cloud mixing ratio predicted by the scheme arise from the use of historical parameters whose applicability to all situations is unknown. According to Reisner et al. (1998), cloud ice may be generated from water vapor by nucleation and deposition. Uncertainty in the nucleation rate results from imposing a minimum temperature to prevent excessive particle concentrations at very cold temperatures. The deposition rate computation is limited to avoid subsaturation with respect to ice. Cloud ice is generated from cloud liquid water by freezing, ice multiplication, and riming. Heterogeneous freezing uncertainty involves a specified value of the num-

ber concentration of cloud drops, while homogeneous freezing uncertainty is linked to setting a specified threshold temperature for occurrence. Ice multiplication is determined by using a fractional factor that is dependent on a specified ambient temperature range. All rimed ice is retained as cloud ice in option 3 of Reisner et al. (1998), not allowing precipitate (graupel), which may lead to excessive cloud ice. The process of converting cloud ice water to precipitating ice water (snow) can have an effect on the simulated precipitation from cirrus and, thus, the amount of ice suspended in the simulated cirrus clouds.

Initial and boundary conditions for the MM5 forecast integration were taken from a 24-h forecast of the Eta Model of the National Centers for Environmental Prediction, acquired from NCAR on a 48-km grid. The 48-km Eta initial conditions were interpolated to the outer MM5 domain to serve as the forecast initial state. After 6 h of integration in the outer domain, the forecast was interpolated to the inner domain, and the forecast continued in both domains until 0000 UTC 23 September 1996. The inner domain forecast fields at 30-min intervals from 1915 to 2345 UTC were compared with the GOES level 2B algorithm retrievals at those same times. No attempt was made to compare MM5 CTH and IWP with radar-derived values because of positioning errors of thunderstorms, found even in storm-scale NWP models by Brewster (1998).

The cloud-top and -base altitudes and IWP are computed at each horizontal grid point in the MM5 forecasts. The predicted ice water mixing ratio in each sigma layer is multiplied by the air density to convert it to mass of water per unit volume of air. The process finds the first sigma layer with a bottom altitude less than 18.1 km that has IWC greater than $\mathrm{IWC}_{\min} = a(10^{-4})^b$, where a and b are taken from Fig. 4 for the predicted sigma layer temperature. The altitude of the top of this sigma layer is designated the CTH. The process continues to search downward until two consecutive sigma layers (having sigma-layer-top altitudes > 6 km) are found with IWC $\leq \mathrm{IWC}_{\min}$. The bottom altitude of the lowest sigma layer above these two layers is designated cloud-base height. The IWP is the product of the sigma-layer IWC and the sigma-layer thickness summed over the sigma layers between CTH and cloud-base height.

Figures 7 and 8 show the CTH and IWP of the GOES level 2B retrievals and MM5 predictions for the first and last comparison times, respectively. Clouds are depicted on the GOES figures only in locations where their tops are at least 6 km in altitude (MM5 tops must be > 6 km, as described in the previous paragraph). The minimum and maximum values in the legends represent the smallest and largest values of the respective quantities found in the 10 comparison times.

In the *GOES-8* depictions, there was a steady eastward march of the strong convection (marked by the highest tops) and accompanying cirrus shields across Florida and the Bahamas. The MM5 convection marches eastward also in the sequence, but starts farther to the west (see Fig. 7b). The accompanying cirrus grows much more extensive in area (46% of grid points) than is depicted in the *GOES-8* figures (32%). The range of CTH is similar for *GOES-8* retrievals and MM5 predictions in this sequence, especially the maximum values. They compare favorably with a tropopause altitude of approximately 16.5 km, measured in a radiosonde sounding at Everglades City that was launched at 2207 UTC.

The retrieved and predicted IWP magnitudes shown in the figures are mostly restricted to the lowest one-fourth of the respective range of values. The MM5 figures show a number of small areas of larger IWP values, while *GOES-8* shows many fewer such areas. The maximum over the entire time sequence is almost one order of magnitude greater for MM5 than for *GOES-8*. For the cloudy points, the average IWP was 85 g m^{-2} for MM5 as compared with 25 g m^{-2} for *GOES-8*. Most of this difference was due to the greater number of small areas of large IWP values in the MM5 predictions. Ninety-eight percent of the GOES-8 cloudy points in the sequence had IWP values of 60 g m^{-2} or less, as compared with 74% for MM5. Ten percent of the MM5 points had values greater than 200 g m^{-2}, as compared with 0.07% of *GOES-8* grid points. The GOES IWP retrievals seem to saturate in larger IWP conditions, as shown in the scan-mode portion of Fig. 6. MM5 is capable of creating ice clouds of significant depth (as great as 8 km in this sequence) comparable to those observed by the CPRS Ka band, as seen in Fig. 5.

6. Summary and conclusions

Cirrus cloud particle probe measurements for two aircraft missions over southern Florida in September 1996 were used to compute ice water content (IWC) and radar reflectivity (Z_e). Separate IWC–Z_e relationships were developed by 6-K ambient temperature regimes. When applied to cloud radar reflectivity observed during the mission periods, these temperature-dependent relationships led to an improved estimation accuracy of IWC, as compared with the use of one relationship for all temperatures.

The radar-inferred IWC was vertically integrated over the depth of the radar-observed cirrus clouds for short-term-averaging periods through the mission periods. The resulting radar-derived cloud-top height (CTH) and ice water path (IWP) were compared with the same quantities retrieved from geostationary satellite imagery by the GOES level-2B algorithm. For a 5-h period in which cirrus of increasing thickness was over the radar site, we found reasonable agreement (no more than 2000-m differences) between the radar- and satellite-retrieved CTHs. However, the retrieved IWP values were smaller than the radar-derived values, especially when the radar-observed cirrus thickness (and corresponding IWP) was greatest. We attributed this difference to the fact that thick cirrus tops are dominated by smaller particle sizes, which with their greater collective

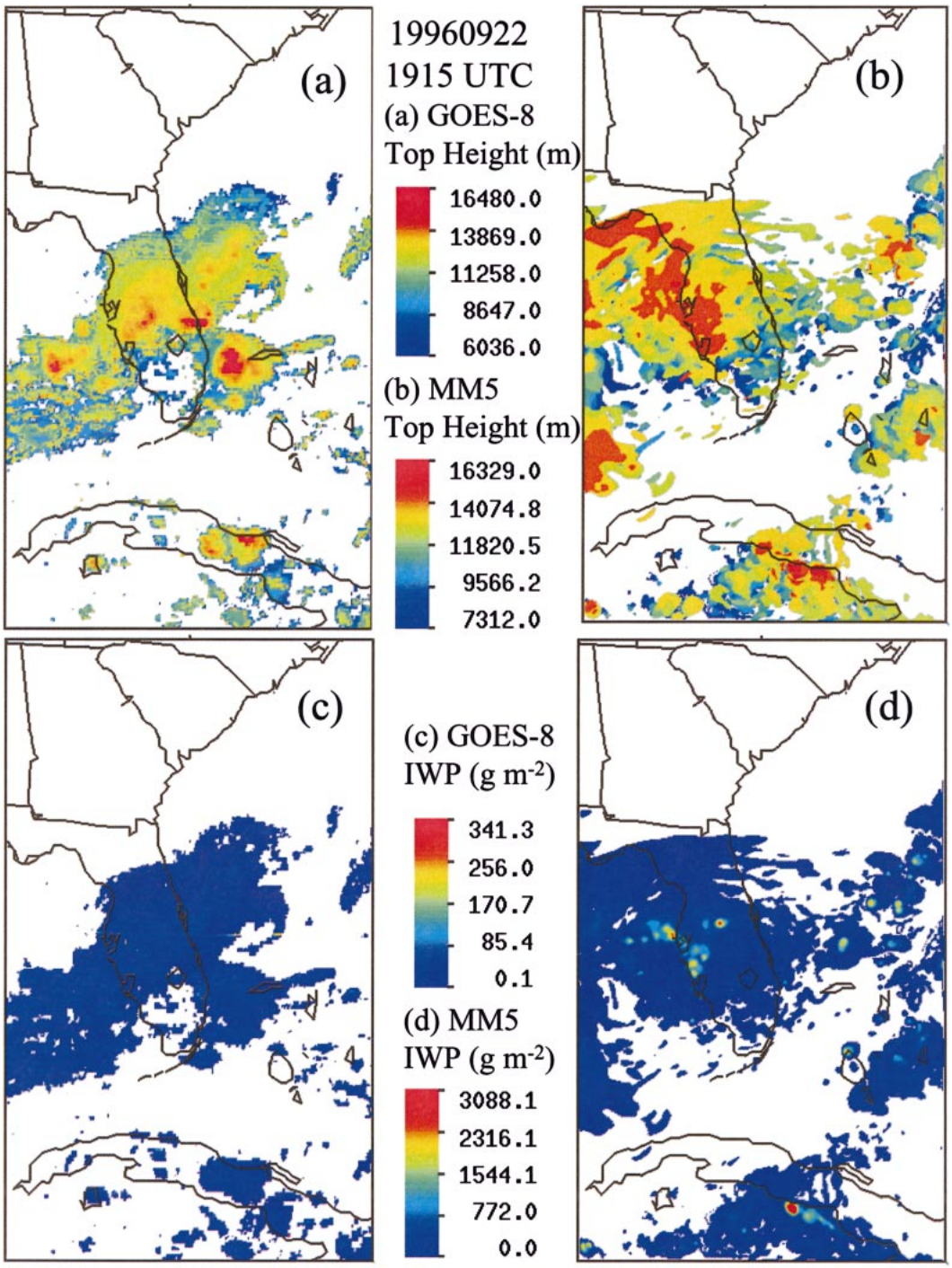

FIG. 7. *GOES-8* retrievals of (a) top height (m) and (c) ice water path (g m^{-2}) compared with MM5 predictions of (b) top height and (d) ice water path for 1915 UTC 22 Sep 1996. Note that the color scales of (c) and (d) are not the same in order to highlight the difference in range between the GOES and MM5 ice water path values over the 10–30-min interval comparison times.

surface area absorb radiation from the particles below and emit to space at their own temperature. Thus, the satellite only ''sees'' the relatively small depth of the smaller particles on the cloud top. This shortcoming of the satellite-based microphysical retrievals of ice clouds at infrared wavelengths effectively limits the use of their retrievals for quantitative evaluation of NWP model–predicted IWP.

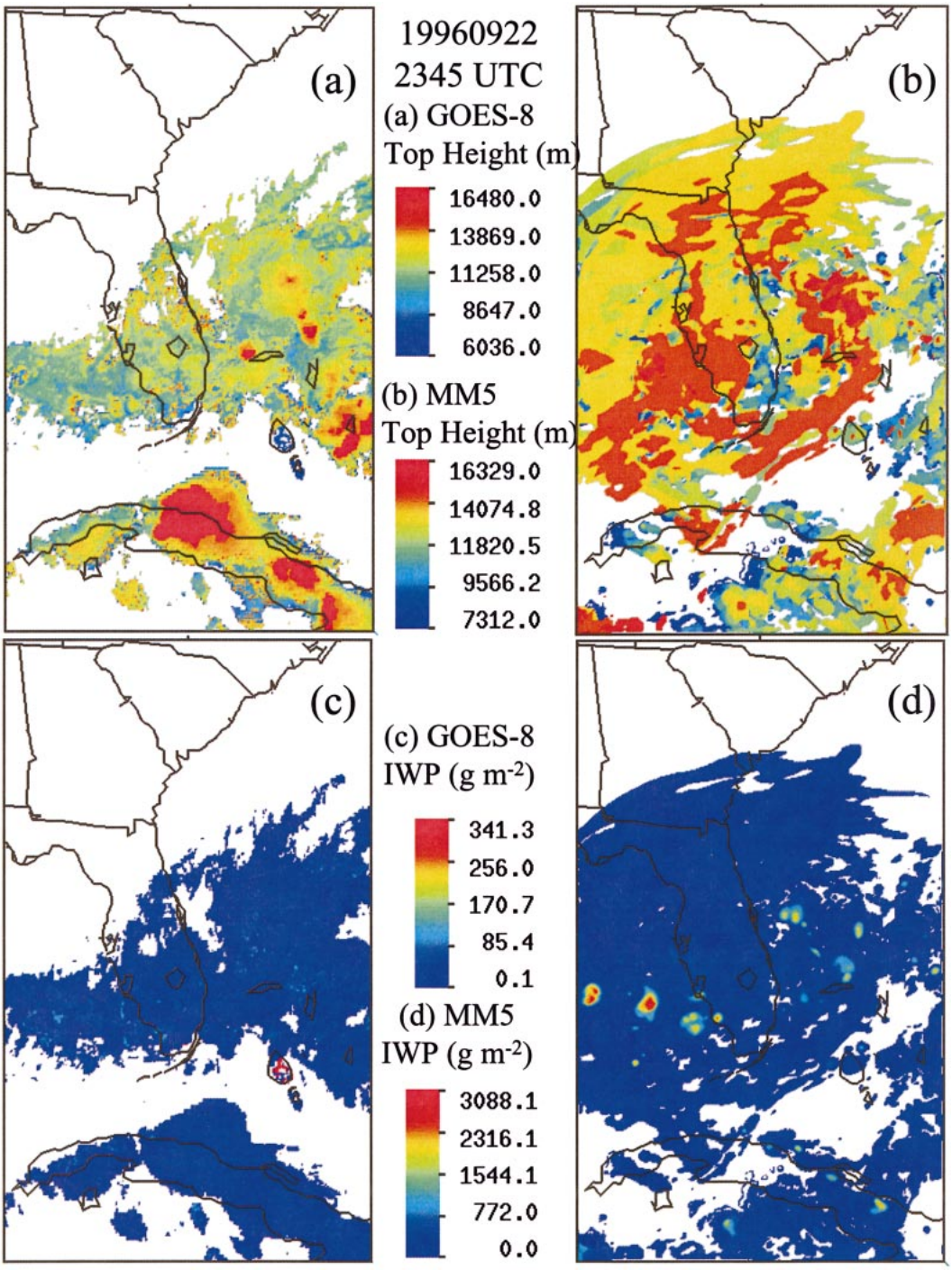

FIG. 8. Same as in Fig. 7, but for 2345 UTC 22 Sep 1996. Color scales for (c) and (d) are the same as their counterparts in Fig. 7 but are not the same as each other.

A sequence of *GOES-8* ice CTH retrievals were compared with MM5-predicted ice cloud tops for a mesoscale area centered on Florida for 22 September 1996. The areal extent of the predicted cirrus was somewhat greater than the satellite depictions throughout the sequence. The range of cloud-top altitudes were similar. Because of the reasonable level of reliability of satellite-retrieved CTH, as validated against cloud radar, we conclude that such depictions are a useful tool for evaluation the distribution of cirrus, as predicted by a mesoscale NWP model.

A different story emerged from the comparisons of

IWP. We found that MM5 is capable of producing significantly large (>1 kg m^{-2}) values of IWP, unlike the satellite retrievals. The maximum value of MM5-predicted IWP was almost one order of magnitude greater than the maximum satellite-retrieved value. The thickness of cirrus is a limiting factor for the passively remote-sensed IWP. Under this constraint, satellite-retrieved IWP does not appear to be a reliable tool for evaluation of predicted IWP.

The conclusions of this study must be tempered by the fact that they are based on a very limited case study. However, we have demonstrated the feasibility of using a collection of different sources of cirrus cloud information to evaluate analyzed and predicted cirrus cloud products. Future work will involve applying these techniques to extensive time series of cloud radar and geostationary imagery, with infrequent calibration of radar measurements with particle probe observations, as available. In addition, we will seek to improve the quality of satellite-based cirrus property retrievals. Ultimately, a satelliteborne cloud radar may improve upon our ability to obtain reliable mesoscale-area retrievals of cirrus properties, which may be of significant value in developing and validating improved cirrus prediction models.

Acknowledgments. We thank Minna Win of NCAR and Kirk Swanson of Aeromet, Inc., for their help in processing the particle probe data. Suggestions for including the effects of 2D-P data by Ray Hobbs of Aeromet were greatly appreciated. Thanks also are due to Anthony Illingworth and Chun-Lei Wu for their guidance in the ice water content and reflectivity computations. We obtained the radar data from Steve Sekelsky at the Microwave Remote Sensing Laboratory, University of Massachusetts. Dan DeBenedictus of Titan Corp. ran the MM5 forecasts. We obtained the Eta Model forecast data from NCAR. Comments from reviewers emphasizing the need to include 2D-P particle sizes in the analysis were helpful. This work was funded by the 6.2 applied research program of the Air Force Research Laboratory.

REFERENCES

Atlas, D., S. Y. Matrosov, A. J. Heymsfield, M.-D. Chou, and D. B. Wolff, 1995: Radar and radiation properties of ice clouds. *J. Appl. Meteor.,* **34,** 2329–2345.

Baumgardner, D., and A. Korolev, 1997: Airspeed corrections for optical array probe sample volumes. *J. Atmos. Oceanic Technol.,* **14,** 1224–1229.

Bohren, C. F., and D. R. Huffman, 1983: *Absorption and Scattering of Light by Small Particles.* John Wiley and Sons, 530 pp.

Brewster, K., 1998: Phase-correcting assimilation of radar data for thunderstorm forecasting. Preprints, *12th Conf. on Numerical Weather Prediction,* Phoenix, AZ, Amer. Meteor. Soc., 181–184.

Brown, P. R. A., A. J. Illingworth, A. J. Heymsfield, G. M. McFarquhar, K. A. Browning, and M. Gosset, 1995: The role of spaceborne millimeter-wave radar in the global monitoring of ice cloud. *J. Appl. Meteor.,* **34,** 2346–2366.

Dudhia, J., 2000: Recent developments and plans for MM5. Preprints, *10th PSU/NCAR Mesoscale Model Users' Workshop,* Boulder, CO, NCAR, 6–8. [Available online at http://www.mmm.ucar.edu/mm5/mm5-home.html.]

Gardiner, B. A., and J. Hallett, 1985: Degradation of in-cloud forward scattering spectrometer probe measurements in the presence of ice crystals. *J. Atmos. Oceanic Technol.,* **2,** 171–180.

Gayet, J.-F., P. R. A. Brown, and F. Albers, 1993: A comparison of in-cloud measurements obtained with six PMS 2D-C probes. *J. Atmos. Oceanic Technol.,* **10,** 180–194.

Grell, G. A., 1993: Prognostic evaluation of assumptions used by cumulus parameterizations. *Mon. Wea. Rev.,* **121,** 764–787.

Gustafson, G. B., and R. P. d'Entremont, 2000: Development and validation of improved techniques for cloud property retrieval from environmental satellites. Air Force Research Laboratory (AFMC) Tech. Rep. AFRL-VS-TR-2001-1549, 56 pp. [Available from AFRL/VSBL, 29 Randolph Rd, Hanscom AFB, MA 01731-3010.]

Hogan, R. J., C. Jakob, and A. J. Illingworth, 2001: Comparison of ECMWF winter-season cloud fraction with radar-derived values. *J. Appl. Meteor.,* **40,** 513–525.

Liu, C.-L., and A. J. Illingworth, 2000: Toward more accurate retrievals of ice water content from radar measurements of clouds. *J. Appl. Meteor.,* **39,** 1130–1146.

Liu, G., and J. A. Curry, 1998: Remote sensing of ice water characteristics in tropical clouds using aircraft microwave measurements. *J. Appl. Meteor.,* **37,** 337–355.

——, and ——, 1999: Tropical ice water amount and its relations to other atmospheric hydrological parameters as inferred from satellite data. *J. Appl. Meteor.,* **38,** 1182–1194.

——, and ——, 2000: Determination of ice water path and mass median particle size using multichannel microwave measurements. *J. Appl. Meteor.,* **39,** 1318–1329.

Mace, G. G., C. Jakob, and K. P. Moran, 1998: Validation of hydrometeor occurrence predicted by the ECMWF model using millimeter wave radar data. *Geophys. Res. Lett.,* **25,** 1645–1648.

Matrosov, S. Y., 1997: Variability of microphysical parameters in high-altitude ice clouds: Results of the remote sensing method. *J. Appl. Meteor.,* **36,** 633–648.

McFarquhar, G. M., and A. J. Heymsfield, 1996: Microphysical characteristics of three anvils sampled during the Central Equatorial Pacific Experiment. *J. Atmos. Sci.,* **53,** 2401–2423.

Morrison, B. J., R. Hobbs, D. Rusk, J. Jung, and R. L. Rose, 1997: The High Altitude Reconnaissance Platform (HARP) SBIRS final report. Aeromet Tech. Rep. AEROMET/TUL 9704211, 264 pp. [Available from Aeromet, Inc., P.O. Box 710767, Tulsa, OK 74170-1767.]

Reisner, J., R. M. Rasmussen, and R. T. Bruintjes, 1998: Explicit forecasting of supercooled liquid water in winter storms using the MM5 mesoscale model. *Quart. J. Roy. Meteor. Soc.,* **124B,** 1071–1107.

Ryan, B. F., 2000: A bulk parameterization of the ice particle size distribution and the optical properties in ice clouds. *J. Atmos. Sci.,* **57,** 1436–1451.

Sekelsky, S. M., W. L. Ecklund, J. M. Firda, K. S. Gage, and R. E. McIntosh, 1999: Particle size estimation in ice-phase clouds using multifrequency radar reflectivity measurements at 95, 33, and 2.8 GHz. *J. Appl. Meteor.,* **38,** 5–28.

Sheu, R.-S., J. A. Curry, and G. Liu, 1997: Vertical stratification of tropical cloud properties as determined from satellite. *J. Geophys. Res.,* **102,** 4231–4245.

Stubenrach, C. J., R. Holz, A. Chedin, D. L. Mitchell, and A. J. Baran, 1999: Retrieval of cirrus ice crystal sizes from 8.3 and 11.1 μm emissivities determined by the improved initialization inversion of TIROS-N Operational Vertical Sounder observations. *J. Geophys. Res.,* **104,** 31 793–31 808.

Young, D. F., P. Minnis, D. Baumgardner, and H. Gerber, 1998: Comparison of in situ and satellite-derived cloud properties during SUCCESS. *Geophys. Res. Lett.,* **25,** 1125–1128.